Electrochimica Acta 54 (2009) 5252–5256

Contents lists available at ScienceDirect

Electrochimica Acta

journal homepage: www.elsevier.com/locate/electacta

Oxygen reduction reaction on carbon-supported $CoSe_2$ nanoparticles in an acidic medium

Yongjun Feng [a], Ting He [b], Nicolas Alonso-Vante [a,*,1]

[a] Laboratory of Electrocatalysis, UMR-CNRS 6503, University of Poitiers, 40 Avenue du Recteur Pineau, 86022 Poitiers, France
[b] Honda Research Institute USA, Inc., Columbus, OH 43212, USA

ARTICLE INFO

Article history:
Received 31 October 2008
Received in revised form 18 February 2009
Accepted 16 March 2009
Available online 28 March 2009

Keywords:
Cobalt selenide nanoparticles
Oxygen reduction reaction (ORR)
Acid medium
Rotating disk electrode (RDE)
Rotating ring-disk electrode (RRDE)

ABSTRACT

We investigated the effect of $CoSe_2$/C nanoparticle loading rate on oxygen reduction reaction (ORR) activity and H_2O_2 production using the rotating disk electrode and the rotating ring-disk electrode techniques. We prepared carbon-supported $CoSe_2$ nanoparticles with different nominal loading rates and evaluated these samples by means of powder X-ray diffraction. All the catalysts had an OCP value of 0.81 V *vs.* RHE. H_2O_2 production during the ORR process decreased with an increase in catalytic layer thickness. This decrease was related to the $CoSe_2$ loading on the disk electrode. H_2O_2 production also decreased with increasing catalytic site density, a phenomenon related to the $CoSe_2$ loading rate on the carbon substrate. The cathodic current density significantly increased with increasing catalytic layer thickness, but decreased with increasing catalytic site density. In the case of 20 wt% $CoSe_2$/C nanoparticles at 22 $\mu g\,cm^{-2}$, we determined that the transfer process involves about 3.5 electrons.

1. Introduction

Since platinum (Pt) is an expensive and exhaustible resource, there is significant interest in the development of non-precious metal electrocatalysts as an alternative for oxygen reduction reaction (ORR) in polymer electrolyte membrane fuel cells (PEMFCs) [1–5]. To date, Pt (33.20 $/g, the average price from 22 September to 22 October 2008 cited from http://www.platinum.matthey.com/prices/price_charts.html) and other Pt-group metals (PGM), e.g., Ru (8.97 $/g), Rh (107.57 $/g), Pd (6.79 $/g), and Ir (14.64 $/g) have been extensively used as ORR electrocatalysts in fuel cell systems. These materials are, unfortunately, among the most expensive and rarest of the metals [2,3,6–9]. Pt-based materials used as ORR catalysts also suffer from slow kinetics, which causes an overpotential ca. 0.3 V, resulting in a large loss in fuel cell efficiency. Other problems with Pt-based catalysts include high sensitivity to contaminants in the feed, e.g., CO, SO_x and NO_x, and low tolerance to methanol oxidation in direct methanol fuel cell (DMFC) systems [10–12].

Choices of a replacement material among non-precious metals are limited due to the metal standard reduction potential, as shown in Fig. 1 [13]. All the PGM metals have a high ORR activity due to their reduction potential, which is closer to the O_2/H_2O reduction potential of 1.23 V *vs.* SHE. Other metals exhibit a potential far more negative than this value. We can see, however, that Co and Fe are promising as cathode catalyst centers. Until now, research has focused primarily on two kinds of non-precious metals for ORR catalysis: metal macrocycles with a catalytic center of Co and Fe, and transition-metal chalcogenides [1,2,4]. The former has been developed since the pioneering work of Jasinski in the 1960s [14,15] on cobalt phthalocyanine. The latter has attracted more attention since Alonso-Vante et al. worked on Chevrel-phase Ru–Mo chalcogenides in the 1980s [16,17]. Recently, some non-precious transition metal chalcogenides, such as $Co_{1-x}Se$/C powder and $Co_{1-x}Se$, MS_2 (M = Co, Fe and Ni) thin films, have shown promising ORR activities [18–20]. These activities are still much lower than Pt-based materials and Ru chalcogenides catalysts. More recently, Bonakdarpour et al. found that the ORR activity and the H_2O_2 release of these systems depends significantly on the carbon-supported ruthenium–selenide loading on the disk electrode [21].

In the present work, we modified the loading of $CoSe_2$ nanoparticles on the electrode surface and on the carbon support to determine its effect on the ORR activity and the H_2O_2 production in an acidic medium. We also examined these results in light of our previous work [22–24].

2. Experimental

2.1 Chemicals

All chemicals, except for the carbon substrate, were used as received from Sigma–Aldrich, Alfa Aesar and Merck without any

* Corresponding author. Tel.: +33 5 4945 3625; fax: +33 5 4945 3580.
E-mail address: Nicolas.Alonso.Vante@univ-poitiers.fr (N. Alonso-Vante).
[1] ISE member.

0013-4686/$ – see front matter © 2009 Elsevier Ltd. All rights reserved.
doi:10.1016/j.electacta.2009.03.052

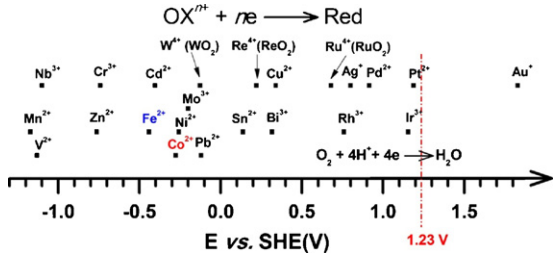

Fig. 1. Standard reduction potential (E°) of metals in aqueous solution. The data are adapted from Ref. [13].

further purification. Vulcan XC-72 carbon, received from CABOT Co., was activated at 400 °C under a high purity nitrogen atmosphere for 4 h before use. Milli-Q Water (18 MΩ cm) was used during the electrochemical measurements.

2.2 In situ free-surfactant synthesis of $CoSe_2$ nanoparticles on carbon supports

Carbon-supported $CoSe_2$ nanoparticles with different nominal loading from 20 wt% to 50 wt% were synthesized by means of the in situ free-surfactant method via conventional heating [22]. For example, to produce 20 wt% $CoSe_2$/C nanoparticles, 0.135 g $Co_2(CO)_8$ (0.395 mmol) and 0.68 g carbon (Vulcan XC-72) were dispersed in 10 mL *p*-xylene with vigorous stirring under a nitrogen atmosphere at room temperature for 30 min. The suspension was heated to the refluxing temperature, then cooled to room temperature without aging. Next, 0.125 g of selenium (1.58 mmol) were dispersed in 8 mL *p*-xylene by ultrasound for 30 min. This dispersion was added to the above suspension of cobalt particles and carbon (*Note: selenium was not completely dissolved in p-xylene*). The resulting suspension was mixed at room temperature for 30 min, then was heated to the refluxing temperature and aged for 10 min. The final black powder was collected on a Millipore filter membrane (dia. 0.22 μm, pore size), washed with anhydrous ethanol and dried under vacuum at room temperature. Other $CoSe_2$/C nanoparticles with different loading ratios were prepared using the same procedure as 20 wt% $CoSe_2$/C nanoparticles, but with an additional amount of carbon substrate corresponding to the desired loading, e.g., 0.318 g carbon for 35 wt% $CoSe_2$/C and 0.171 g carbon for 50 wt% $CoSe_2$/C. All of the $CoSe_2$/C nanoparticle samples were treated at 300 °C under a high purity nitrogen atmosphere for 3 h before characterization.

2.3 Characterization techniques

Powder X-ray diffraction (PXRD) was performed on a Bruker D5005 diffractometer under the following conditions: 40 kV, 40 mA Cu Kα (λ = 1.5418 Å) radiation. The samples, as non-oriented powder, were step-scanned in steps of 0.03° (2θ) in the range of 20–70° using a counter time of 5 s per step.

All electrochemical measurements were conducted at 25 °C in a thermostated three compartment electrochemical cell. All the potentials in this paper are reported *vs.* a reversible hydrogen electrode (RHE) in 0.5 M H_2SO_4 aqueous solution. The rotating disk electrode (RDE) measurements were performed at 25 °C using a potentiostat (μ-Autolab Type II). The working electrode was a glassy carbon disk with a 3.0 mm diameter (0.07 cm^2). The catalyst ink was prepared by dispersing 4 mg powder in a mixture of 250 μL Nafion® solution (5 wt% in mixture of lower aliphatic alcohols and water, Aldrich) and 1250 μL ultrapure water (18 mΩ cm) in an ultrasonic bath for 2 h. After polishing the glassy carbon disc with Al_2O_3 powder (5A), a 3 μL drop of catalyst ink was deposited on its surface. Aqueous 0.5 M H_2SO_4 was used as an electrolyte. Glassy carbon and home-made reference hydrogen electrodes were used as the counter, and reference electrodes, respectively. The reference electrode was separated from the working electrode compartment by an electrolyte bridge with a Luggin capillary. Before the electrochemical measurements, the electrolyte was deaerated by bubbling nitrogen through it for 30 min. The electrode was subjected to 10 cycles of cyclic voltammetry from 0.80 V to 0.05 V under a high purity nitrogen atmosphere to clean the surface. Following this cleaning, linear-sweep voltammograms were recorded by scanning the disk potential *vs.* RHE at 5 mV s^{-1} at rotating speeds of 400, 900, 1225, 1600 and 2500 rpm.

The rotating ring-disk electrode (RRDE) measurements were conducted at 25 °C using an interchangeable ring-disk electrode setup with a bi-potentiostat (Autolab PGSTAT 30) and a rotation control system (Pine Instruments). The Pt ring electrode (0.152 cm^2, area) was potentiostated at 1.2 V, where the detection of peroxide is diffusion limited. The disk electrode was glassy carbon with an area of 0.162 cm^2. The counter and the reference electrodes were the same as in the RDE experiments.

3. Results and discussion

3.1 Structural and loading detection of carbon-supported $CoSe_2$ nanoparticles

Fig. 2 shows powder X-ray diffraction (PXRD) patterns after background subtraction of $CoSe_2$/C with different nominal loading from 20 wt% to 50 wt% at a fixed weight of 16.5 mg. All samples displayed the typical crystalline characteristics of orthorhombic $CoSe_2$ (relative to ICDD-PDF 2004-00-53-0449, marked at the bottom with red dot-dashed lines. The (1 1 1) Bragg reflection peak is centered at ca. 34.4°/2θ and has the highest intensity among these reflection peaks. There is a well-known linear relationship between the reflection intensity, or integrated area of a certain Bragg peak, and the amount of the associated phase in a multiphase mixture. Here, we selected the (1 1 1) Bragg reflection peak as the objective peak and integrated the corresponding area in the range from 33.8° to 35.0°/2θ. Fig. 3 demonstrates an almost linear relationship between the integrated area of the (1 1 1) Bragg reflection peak and

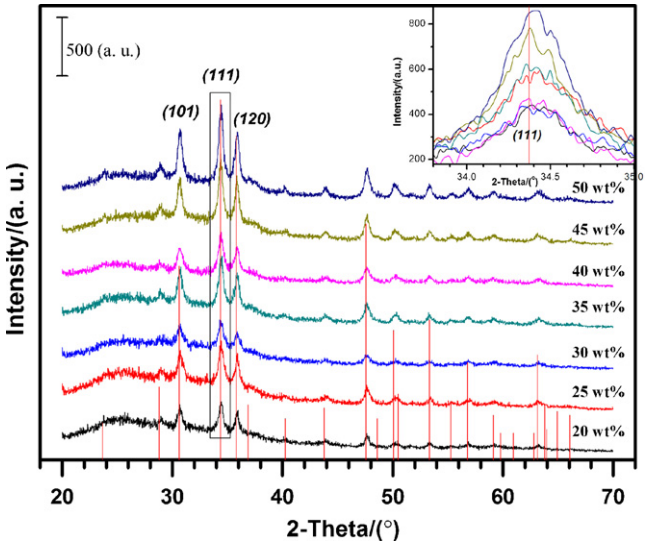

Fig. 2. Powder X-ray diffraction patterns of carbon-supported $CoSe_2$ nanoparticles after background subtraction. All samples weighed 16.5 mg and were subjected to heat treatment at 300 °C under high purity nitrogen for 3 h. Nominal loading was varied from 20 wt% to 50 wt%. Vertical dot-dashed lines represent the ICDD-PDF2-2004 card of $CoSe_2$ No. 00-053-0449. The inset shows the integrated peak in the range from 33.8° to 35.0°/2θ.

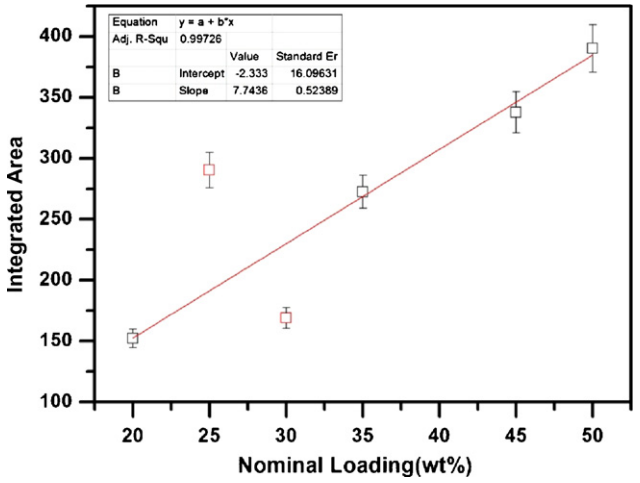

Fig. 3. Linear fit of the integrated area of the $CoSe_2$-associated (1 1 1) Bragg reflection *vs.* the nominal loading of $CoSe_2$ on carbon. The adjusted *R*-squared value is 0.997 and the error bars represent 5% uncertainty.

the nominal loading, with an adjusted *R*-squared value of 0.997. The 20 wt%, 35 wt%, and 50 wt% points fall on the best fit line. However, the nominal loading of 30 wt% was approximately equal to the result for 20 wt% and the nominal loading of 25 wt% is close to the result for 35 wt%, based on calculation of the integrated area. This result indicates that the synthesis conditions should be carefully controlled in order to obtain the exact desired $CoSe_2$ nanoparticle loading. Therefore, we mainly focused on the 20 wt%, 35 wt%, and 50 wt% $CoSe_2$/C samples in the following electrochemical investigation.

3.2 ORR activity of 20 wt% $CoSe_2$/C nanoparticles

The Koutecky–Levich plot (Fig. 4) shows a linear and parallel relationship at 0.40 V, 0.30 V, and 0.20 V, indicating first-order kinetics for molecular oxygen. This Koutecky–Levich plot was obtained from the ORR curves based on the Koutecky–Levich equation as follows:

$$\frac{1}{i} = \frac{1}{i_k} + \frac{1}{i_d} = \frac{1}{i_k} + \frac{1}{B\omega^{1/2}} \quad (1)$$

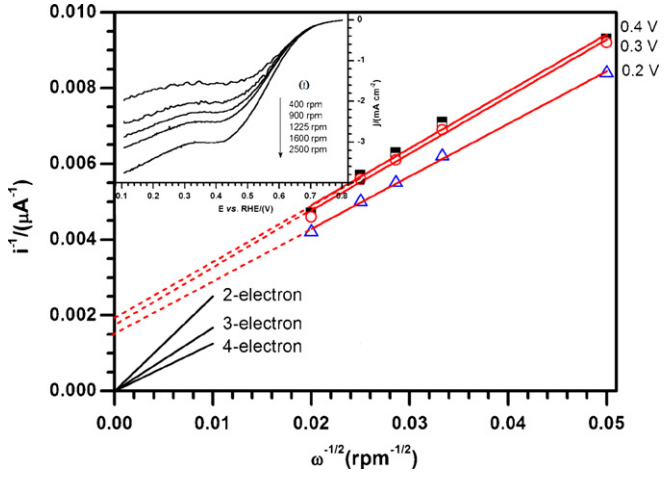

Fig. 4. Koutecky–Levich plots and ORR curves collected on glassy carbon electrodes under O_2-saturated 0.5 M H_2SO_4 at 25 °C for samples with 20 wt% $CoSe_2$/C nanoparticles (inset on the top). The loading of $CoSe_2$ nanoparticles on the electrode was 22 μg cm^{-2} and the scan rate was 5 mV s^{-1}. The lines on the bottom are drawn for 2-, 3- and 4-electron transfer pathways, respectively.

where i, i_k, i_d are total, kinetic and diffusion current, respectively, and ω is the angular velocity. B is a constant equal to $0.2nFAD^{2/3}\nu^{-1/6}C_{O2} \approx 2n$ μA rpm$^{-1/2}$, where $F = 96{,}500$ C, $A = 0.07$ cm^2, $D = 1.40 \times 10^{-5}$ cm^2 s^{-1}, $\nu = 0.01$ cm^2 s^{-1} and $C_{O2} = 1.1 \times 10^{-6}$ mol cm^{-3} under similar experimental conditions [25]. We calculated the slope (B^{-1}) of 0.14 ± 0.01 μA^{-1} rpm$^{1/2}$ from a function of i^{-1} *vs.* $\omega^{-1/2}$ at three potentials. From this slope we can derive the number of electrons transferred during the reduction of an oxygen molecule. Using this method, we calculated a transfer of about 3.5 electrons, compared to the theoretical result of between 3 and 4 electrons.

The inset plot illustrates the presence of a plateau-like cathodic diffusion current in the range from 0.1 V to 0.44 V. The cathodic current density of ca. 2.5 mA cm^{-2} at 0.4 V at 1600 rpm was comparable to results reported in the literature from non-precious metal electrocatalysts [18–20]. Examples of some such results are 2.0 mA cm^{-2} for $Co_{1-x}Se$/C powder catalysts (50 wt% Cobalt on XC-72R carbon) [18], and 2.5 mA cm^{-2} for (Co, Ni)S_2 thin films [20] at 2000 rpm. The OCP value of 0.81 V in O_2-saturated 0.5 M H_2SO_4 was slightly higher than that of $Co_{1-x}Se$/C powder catalysts (0.78 V), $Co_{1-x}Se$ ($x = -1.5$, 0 and 0.23; 0.74 V) [18], and FeS_2 (0.78 V) thin films [19]. This value was similar to that of NiS_2 (0.80 V), and CoS_2 (0.82 V) thin films [20], but lower than that of (Co, Ni)S_2 (0.89 V) thin films [20].

Here, the ORR curves showed two times higher current density than reported in our previous work with 20 wt% $CoSe_2$/C nanoparticles at the same rotating speed [22]. This enhancement resulted from the twofold higher loading of $CoSe_2$ nanoparticles (11 μg cm^{-2} in Ref. [22] and 22 μg cm^{-2} in the present work) on the glassy carbon electrode. Recently, it was reported that a loading increase of 20 wt% Ru_xSe_y/C on the disk electrode from 5 to 92 μg cm^{-2} results in an increase in cathodic current density from 2 mA cm^{-2} to 5.8 mA cm^{-2} [21]. Therefore, we further investigated the influence of the disk electrode loading rate of $CoSe_2$ catalyst on the ORR activity and on hydrogen peroxide production during the ORR process.

Fig. 5 shows the ring and the disk current as a function of potential from 0.82 V to 0.10 V for different loadings of $CoSe_2$ on the disk electrode from 11 μg cm^{-2} to 44 μg cm^{-2}. All samples had a ratio of 20 wt% $CoSe_2$ in carbon. Four electrodes were prepared by individual deposition of 3.47 μL, 6.94 μL, 10.41 μL, and 13.88 μL of the

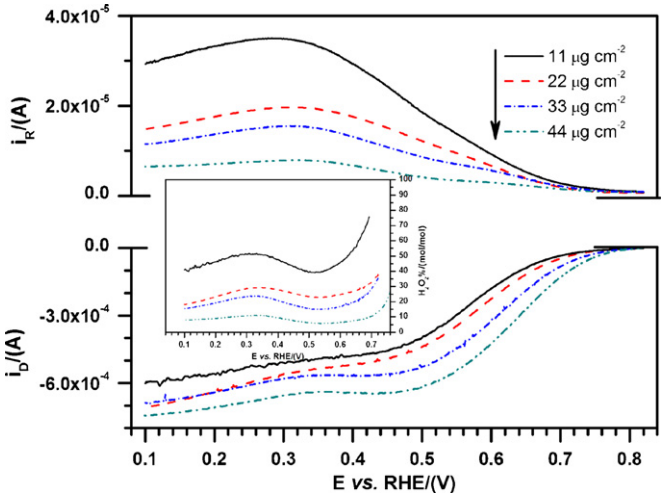

Fig. 5. ORR currents and fraction of H_2O_2 formation (inset) for 20 wt% $CoSe_2$/C catalyst in the O_2-saturated 0.5 M H_2SO_4 recorded at 5 mV s^{-1}, 2500 rpm, and 25 °C. The loading of $CoSe_2$ nanoparticles on the disk electrode was 11 μg cm^{-2} (solid line), 22 μg cm^{-2} (dashed line), 33 μg cm^{-2} (short dashed–dotted line) and 44 μg cm^{-2} (dashed–dotted–dotted line) as indicated. The fraction of H_2O_2 formation was calculated according to Eq. (2) with a collection efficiency $N = 0.21$.

same ink on a disk electrode of area 0.162 cm^2. This ink consisted of 4 mg 20 wt% $CoSe_2$/C powder, 1250 μL Millipore water and 250 μL Nafion® solution. Performing ORR on the $CoSe_2$/C disk surface produces H_2O_2 that is oxidized to O_2 at the Pt ring surface. Increasing the loading rate from 11 μg cm^{-2} to 44 μg cm^{-2} increased the disk current density (intensity) at 0.5 V from 2.5 mA cm^{-2} (0.4 mA) to 3.8 mA cm^{-2} (0.62 mA). In contrast, the ring current intensity decreased with a catalyst loading increase. As noted in Figs. 4 and 5, the shape of the ORR current–potential curves at a potential lower than 0.65 V indicates that this reaction is dominated by a mixed kinetic/diffusion control.

The inset graph (Fig. 5) shows the mol fraction of H_2O_2 formation (X_{H2O2}) during the ORR process. This fraction can be calculated from the molar flux of O_2 and H_2O_2 according to the following Eq. (2) based on the ring and disk current [26]:

$$H_2O_2\% = \frac{200 \times I_R/N}{I_D + I_R/N} \quad (2)$$

where N is collection efficiency, 0.21. The maximum H_2O_2% production (at ca. 0.32 V) in the range from 0.60 V to 0.10 V was 50%, 30%, 23%, and 10% for 11–44 μg cm^{-2}, respectively. Ahlberg and Elfström Broo performed a similar study for pyrite in the pH range of 2–10. They found ca. 25–30% H_2O_2 production at the disk electrode, which was detected at the ring electrode during the ORR process[27].

The catalyst loading effect with respect to H_2O_2 production can be understood in terms of an increase in the catalytic layer thickness. In a thicker layer, the hydrogen peroxide molecule has additional time to chemically react to water. This increased reaction results in an increase in the overall number of electrons as well as a decrease in H_2O_2 detected at the ring electrode.

3.3 Influence of $CoSe_2$ loading on ORR activity and H_2O_2 production

Fig. 6 displays the influence of 20 wt%, 35 wt%, and 50 wt% $CoSe_2$/C loading of nanoparticles on the ORR activity and on the H_2O_2 production during the ORR process at 2500 rpm and 25 °C. We prepared these three electrodes identically. For each electrode, we dispersed 4 mg of carbon-supported $CoSe_2$ powder in 1250 μL Millipore water and 250 μL Nafion® solution. We then deposited 6.94 μL of this ink on a disk electrode of area 0.162 cm^2. Because of these identical processing conditions, we can assume that the catalytic layer has the same thickness in each sample. Therefore, we can relate the different catalytic site density in the catalytic layer to the various $CoSe_2$ loading rates on the carbon substrate. The maximum H_2O_2 production at the ring electrode decreases from 30% to 15% when the loading rate is changed from 20 wt% $CoSe_2$/C to 50 wt% $CoSe_2$/C. There may be a catalytic site density limit since 35 wt% and 50 wt% $CoSe_2$/C catalysts released a similar percentage of H_2O_2 during oxygen reduction. The disk cathodic current density (intensity) at 0.4 V decreased from 3.4 mA cm^{-2} (0.55 mA) to 2.2 mA cm^{-2} (0.35 mA) with an increase from 20 wt% to 50 wt% $CoSe_2$/C. A similar trend has been observed with 20 wt% Ru/Se/C, which has higher disk current density than 70 wt% Ru/Se/C [21].

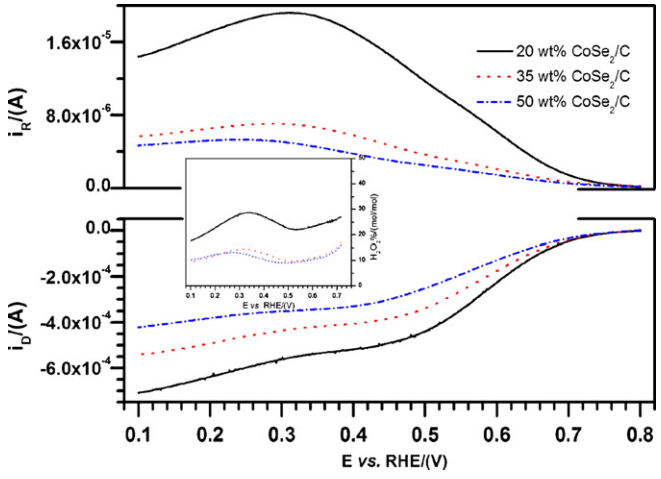

Fig. 6. ORR currents and fraction of H_2O_2 formation (inset) for 20 wt%, 35 wt% and 50 wt% $CoSe_2$/C catalyst in the O_2-saturated 0.5 M H_2SO_4 recorded at 5 mV s^{-1}, 2500 rpm, and 25 °C. The loading of $CoSe_2$ nanoparticles on the disk electrode was 22 μg cm^{-2} for 20 wt% (solid line), 38.5 μg cm^{-2} for 35 wt% (dotted line), and 55 μg cm^{-2} for 50 wt% (short dashed–dotted line). The fraction of H_2O_2 formation was calculated according to Eq. (2) with a collection efficiency N = 0.21.

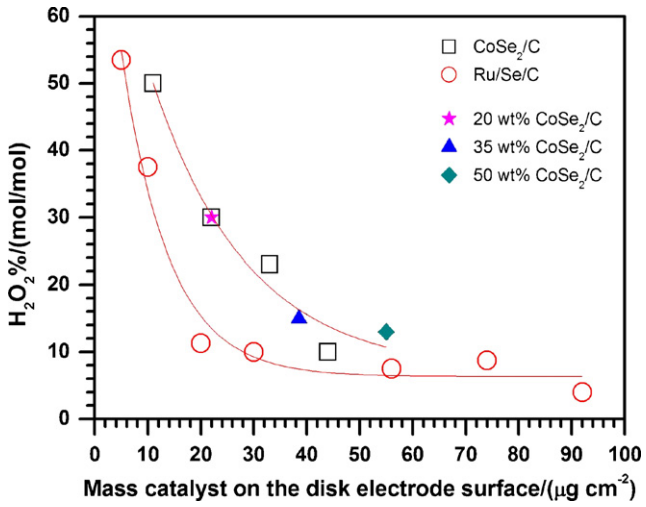

Fig. 7. H_2O_2 mol fraction as a function of the mass of catalyst per unit surface. The data corresponding to the $CoSe_2$/C systems were extracted from insets of Figs. 5 and 6. For the ruthenium–selenide system, data were extracted from Ref. [21]. The mass of catalyst was varied from 20 wt% $CoSe_2$/C. Data for Ru–Se/C were obtained for the same catalyst/carbon ratio. Full symbols represent $CoSe_2$/C with three different catalyst/carbon ratios.

3.4 Understanding the effect of the catalyst loading on the production of H_2O_2

As shown in Fig. 5, increasing the mass of catalyst per unit surface leads to an increase in the molecular oxygen reduction current with a concomitant decrease in hydrogen peroxide production according to the reaction:

$$H_2O_2 + 2H^+ + 2e^- \rightarrow 2H_2O \quad (3)$$

On the other hand, increasing the loading rate from 20 wt% to 50 wt% also leads to a decrease in hydrogen peroxide production. However, the ORR reduction current decreases, as shown in Fig. 6. Both results, which at first seem contradictory, can be rationalized by plotting the molar fraction of hydrogen peroxide as a function of the mass of catalyst loading per unit surface. This comparison is shown in Fig. 7. If we assume that the layer thickness (produced by a consequent deposition of catalyst, as shown in Fig. 5) does not play an important role, we arrive at the conclusion that an increase in the number of catalytic sites (or mass surface density) is necessary to produce the higher reaction rate (3). This feature was also encountered when analyzing data from Ref. [21]. This variation with catalytic site density in the release rate of H_2O_2 into the electrolyte has to be taken into account for practical systems.

4. Conclusions

We have investigated the influence of $CoSe_2$ nanoparticle loading on the carbon substrate and on the glassy carbon disk electrode

surface on the oxygen reduction reaction and the H_2O_2 production in a 0.5 M H_2SO_4 electrolyte. We performed these detailed investigations with the rotating disk electrode and rotating ring-disk electrode techniques. The ORR activity and H_2O_2 production depended on the catalytic layer thickness and on the catalytic site density. Carbon-supported $CoSe_2$ nanoparticles have shown promise as non-precious metal electrocatalysts, with an OCP value of 0.81 V *vs.* RHE and a possible four-electron transfer mechanism. Currently, H_2O_2 production is still higher than the requirement (below 5%) for polymer electrolyte membrane fuel cell systems and the ORR activity is still lower than that of Pt- or Ru-based catalysts. We plan further investigation to improve the ORR multi-electron charge transfer and to reduce H_2O_2 production. This future work will focus on ways to modify the $CoSe_2$ nanoparticle surface and methods to reduce $CoSe_2$ particle size.

Acknowledgments

This work was supported by the Honda Research Institute USA and the University of Poitiers.

References

[1] C.W.B. Bezerra, L. Zhang, K. Lee, H. Liu, A.L.B. Marques, E.P. Marques, H. Wang, J. Zhang, Electrochim. Acta 53 (2008) 4937.
[2] Y.J. Feng, N. Alonso-Vante, Phys. Status Solidi B 245 (2008) 1792.
[3] J.-W. Lee, B.N. Popov, J. Solid State Electrochem. 11 (2007) 1355.
[4] L. Zhang, J. Zhang, D.P. Wilkinson, H. Wang, J. Power Sources 156 (2006) 171.
[5] B. Wang, J. Power Sources 152 (2005) 1.
[6] C.W.B. Bezerra, L. Zhang, H. Liu, K. Lee, A.L.B. Marques, E.P. Marques, H. Wang, J. Zhang, J. Power Sources 173 (2007) 891.
[7] E. Antolini, J.R.C. Salgado, E.R. Gonzalez, J. Power Sources 160 (2006) 957.
[8] J. Zhang, M.B. Vukmirovic, K. Sasaki, A.U. Nilekar, M. Mavrikakis, R.R. Adzic, J. Am. Chem. Soc. 127 (2005) 12480.
[9] H.A. Gasteiger, S.S. Kocha, B. Sompalli, F.T. Wagner, Appl. Catal. B: Environ. 56 (2005) 9.
[10] J. Zhang, F.H.B. Lima, M.H. Shao, K. Sasaki, J.X. Wang, J. Hanson, R.R. Adzic, J. Phys. Chem. B 109 (2005) 22701.
[11] A.K. Shukla, R.K. Raman, Annu. Rev. Mater. Res. 33 (2003) 155.
[12] R. Borup, J. Meyers, B. Pivovar, Y.S. Kim, R. Mukundan, N. Garland, D. Myers, M. Wilson, F. Garzon, D. Wood, P. Zelenay, K. More, K. Stroh, T. Zawodzinski, J. Boncella, J.E. McGrath, M. Inaba, K. Miyatake, M. Hori, K. Ota, Z. Ogumi, S. Miyata, A. Nishikata, Z. Siroma, Y. Uchimoto, K. Yasuda, K.i. Kimijima, N. Iwashita, Chem. Rev. 107 (2007) 3904.
[13] J.G. Speight, Lange's Handbook of Chemistry, 16th ed., McGraw-Hill, New York, 2005.
[14] R. Jasinski, J. Electrochem. Soc. 112 (1965) 526.
[15] R. Jasinski, Nature 201 (1964) 1212.
[16] N. Alonso-Vante, H. Tributsch, Nature 323 (1986) 431.
[17] N. Alonso-Vante, W. Jaegermann, H. Tributsch, W. Hoenle, K. Yvon, J. Am. Chem. Soc. 109 (1987) 3251.
[18] D. Susac, A. Sode, L. Zhu, P.C. Wong, M. Teo, D. Bizzotto, K.A.R. Mitchell, R.R. Parsons, S.A. Campbell, J. Phys. Chem. B 110 (2006) 10762.
[19] D. Susac, L. Zhu, M. Teo, A. Sode, K.C. Wong, P.C. Wong, R.R. Parsons, D. Bizzotto, K.A.R. Mitchell, S.A. Campbell, J. Phys. Chem. C 111 (2007) 18715.
[20] L. Zhu, D. Susac, M. Teo, K.C. Wong, P.C. Wong, R.R. Parsons, D. Bizzotto, K.A.R. Mitchell, S.A. Campbell, J. Catal. 258 (2008) 235.
[21] A. Bonakdarpour, C. Delacote, R. Yang, A. Wieckowski, J.R. Dahn, Electrochem. Commun. 10 (2008) 611.
[22] Y.J. Feng, T. He, N. Alonso-Vante, Chem. Mater. 20 (2008) 26.
[23] Y.J. Feng, T. He, N. Alonso-Vante, ECS Trans. 11 (2008) 67.
[24] Y.J. Feng, T. He, N. Alonso-Vante, Fuel Cells (2009), submitted for publication.
[25] K.-L. Hsueh, E.R. Gonzalez, S. Srinivasan, Electrochim. Acta 12 (1983) 691.
[26] U.A. Paulus, T.J. Schmidt, H.A. Gasteiger, R. J. Behm, J. Electroanal. Chem. 495 (2001) 134.
[27] E. Ahlberg, A. Elfström Broo, Int. J. Miner. Process. 46 (1996) 73.